Available online at www.sciencedirect.com
SCIENCE DIRECT®
Composite Structures 68 (2005) 185–202
COMPOSITE STRUCTURES
www.elsevier.com/locate/compstruct

Bending of composites and sandwich plates subjected to localized lateral loadings: a comparison of various theories

Erasmo Carrera *, Angelo Ciuffreda

Department of Aeronautics and Aerospace Engineering, Politecnico di Torino, Corso Duca degli Abruzzi 24, 10129 Torino, Italy

Available online 15 April 2004

Abstract

A unified compact formulation of theories for multilayered structures analyses, that has recently been proposed by the first author, is, in this paper, extended to study the response of composites and sandwich plates subjected to localized distribution of transverse pressure and to point loadings. Closed form 'exact' solutions are presented by expanding the applied loadings in Fourier series. Relevant plate theories are compared. These theories cover the most significant aspects of two-dimensional modeling of layered structures: layer-wise and equivalent single layer variable descriptions are compared; classical models formulated with only displacement unknowns are compared to advanced ones that were obtained by employing the Reissner mixed variational theorem. Furthermore, the considered plate theories permit to evaluate the effect of both zig-zag form of the displacement field in the thickness plate direction and interlaminar continuity of transverse shear and normal stresses to be evaluated, as well as the role played by the transverse normal strain to be assessed.

Four distinct benchmarks were examined in the numerical investigation: BM1 is related to a sandwich plate loaded by uniform distribution of transverse pressure on the top surface; BM2 and BM3 restrict the application of the transverse pressure of the BM1 case to a smaller areas located in the center of the plate; BM4 is related to a three layered plate subject to point loading.

The stress and displacement fields in the vicinity of the loaded areas were compared to three-dimensional elasticity solutions and to available finite element analyses. It has been concluded in particular that: the issues that are already know for classical problems require amendment if localized loadings problems are analyzed; layer-wise analyses are required to capture localized stress/fields in the neighborhood of the loading area; transverse normal deformation must be taken into account to accurately predict behaviors of the sandwich core.

Keywords: Multilayered structures; Sandwich plates; Classical theories; Advanced theories; Localized loadings; Closed form solutions

1. Introduction

Laminated composites and sandwich structures combine light weight with high stiffness, high structural efficiency and durability, and have therefore been widely used to build large portions of aerospace, automotive, and ship structures. The high performance of these multilayered structures makes them ideal candidates for use in future high speed aircraft, spacecraft, satellite antennas and terrestrial systems reflector. As far as the two-dimensional modelings of multilayered flat structures is concerned, whose developments this paper is devoted, there are a number of requirements that should be considered for an accurate description of their stress and strain fields. Among these: (1) anisotropic multilayered structures often possess higher transverse shear and normal flexibility than the traditional isotropic one-layer ones; (2) the intrinsic discontinuity of the mechanical properties in the thickness plate direction demands the description of the so-called zig-zag (ZZ) form of displacement field in the thickness direction and interlaminar continuity (IC) of the transverse shear and normal stresses. These two points are of extreme importance in the case of sandwich panels, whose core deformability is at least one order of magnitude higher than that of the faces.

Many refinements of classical models have been proposed to overcome the limitations of well known classical plate models, such as CLT and FSDT analyses

* Corresponding author. Tel.: +39-011-546-6836/564-6836; fax: +39-011-564-6899.
E-mail addresses: erasmo.carrera@polito.it, carrera@polito.it (E. Carrera).

0263-8223/$ - see front matter © 2004 Elsevier Ltd. All rights reserved.
doi:10.1016/j.compstruct.2004.03.013

Nomenclature

Symbols and acronyms which are used in places distant from their definition are listed below

a, b, h plate geometrical parameters (length, width and thickness)
k sub/super-script used to denote parameters related to the k-layer
N order of the expansions used for transverse stresses and displacements
N_l number of constituent layers of multilayered plate
P_z, p_{zT} amplitude of point loading and transverse pressure, respectively
R, Q order of the Fourier expansion in Eq. (14)
x, y, z coordinates of Cartesian reference systems used for plates
V plate volume
Ω plate reference surface
Ω_{BM1}, Ω_{BM2}, Ω_{BM3} top surface areas on which transverse pressure p_{zT} is applied for BM1, BM2, BM3 analyses, respectively
2D, 3D two dimensional, three dimensional analyses, respectively
BM1, BM2, BM3, BM4 benchmark problems described in Section 5
CLT classical lamination theory
ESLM equivalent single layer models
ED1, ED4 ESLM based on PVD applications with $N = 1$ and 4, respectively
ED1d ED1 sub-case which neglects transverse normal strain
EMZC3 ESLM theory based on RMVT with $N = 3$, fulfilling ZZ and IC
EMZC3d EMZC3 which neglects transverse normal strain
Err-3D, Err-LD4 averaged error to 3D and LM4 analyses, respectively
FEM finite element method
FSDT first order shear deformation theory
IC interlaminar continuity
LM2, LM4 LWM theories based on RMVT with $N = 2$, 4, respectively
LWM layer-wise models
PVD principle of virtual displacements
RMVT Reissner's mixed variational theorem
ZZ zig-zag

as well as to include ZZ and IC [1–3]. Classical models with only displacement unknowns as well as advanced models based on mixed assumptions have been developed in both the ESLM and LWM variables description framework [4]. Following Reddy [3], it is understood that ESLMs preserve the independence of the number of the independent variables from the number of the N_l-layers while the number of the unknown variables remains N_l-dependent in the LWM cases. A complete discussion of the several contributions that have appeared in literature has been covered by recent exhaustive state-of-art articles. Among these one can mention papers [5–18].

The numerical assessment of available plate theories has mostly been restricted to problems for Pagano gave 3D elasticity solutions [19,20]. These benchmark problems are related to sandwich and composites plates with various geometries, bent by transverse distribution of pressure applied over the whole top/bottom plate surface.

In most of the practical applications of multilayered structures, loads are applied to localized regions. The assessment of classical and advanced plate theories vs localized loading problems could therefore be of interest for structural analysts. Interest in additional benchmarking is also displayed by the recent articles by Meyer-Piening [22], Meyer-Piening and Stefanelli [21], Barut et al. [24], Anderson et al. [23] and by Carrera and Demasi [25].

The present work aims of contributing to this subject by giving closed form solutions for sandwich and composites plates subjected to various localized loadings. Additional benchmark problems are therefore proposed and relevant plate theories are compared. Four benchmark problems (BM1–BM4) are investigated: three of these are related to a moderately thick sandwich plate subjected to three different loading cases, the latter deals with a point load problem applied to a cross-ply plate. As far as the considered plate theories is concerned, reference is made to the unified formulations proposed by the first author in [4,16,18]. Classical modelings based on displacement assumptions as well as mixed theories which assume both displacement and transverse stress variables are considered. RMVT and PVD are referred to in order to derive governing equations. LWM and ESLM are developed including and/or discarding ZZ and IC effects. Linear up-to forth order thickness expansions are implemented for the unknown variables. The effect of transverse normal strain is evaluated. The Navier-type closed form solutions that was restricted to harmonic distributions of transverse pressures in a previous work [16], has here been extended to BM1–BM4 problems. This is done by expanding the constant distribution of transverse

pressure as well as concentrated loadings, in terms of appropriate Fourier series.

This paper has been organized as follows. Section 2 briefly describes the selected 2D mechanical models that are used in the numerical part. Section 3 details on the compared theories. Section 4 outlines the governing differential equations and the related closed form solutions. Section 5 describes the four benchmarks that we investigated. The evaluations and discussion are given in Section 6.

2. Mechanics of the 2D modelings

According to what was described in [16] 2D models of multilayered plates have been developed by making assumptions in the thickness directions z (see Fig. 1). Displacements $\mathbf{u}$ and transverse stresses $\boldsymbol{\sigma}_n$ are the variables that are represented by the following formulas,

$$\begin{aligned} \mathbf{u} &= F_t\mathbf{u}_t + F_b\mathbf{u}_b + F_r\mathbf{u}_r = F_\tau\mathbf{u}_\tau, \\ \boldsymbol{\sigma}_n &= F_t\boldsymbol{\sigma}_{n_t} + F_b\boldsymbol{\sigma}_{n_b} + F_r\boldsymbol{\sigma}_{n_r} = F_\tau\boldsymbol{\sigma}_{n_\tau}, \\ \tau &= t, b, r, \quad r = 2, \ldots, N \end{aligned} \tag{1}$$

Bold letters denote arrays ($\mathbf{u} = \{u_x, u_y, u_z\}$, $\boldsymbol{\sigma}_n = \{\sigma_{xz}, \sigma_{yz}, \sigma_{zz}\}$, and so on). A Cartesian reference system is referred to. F_t, F_b and F_r are the base functions used for the z-expansions, the first two polynomials are related to the linear part of such expansions, while F_r introduced the $N-1$ higher order terms (power of z and Legendre polynomials are used to build up F_t, F_b and F_r in the case of LW and ESLM, respectively). The same meaning is assumed by the related introduced variables $\mathbf{u}_t$, $\mathbf{u}_b$, $\mathbf{u}_r$, $\boldsymbol{\sigma}_{nt}$, $\boldsymbol{\sigma}_{nb}\boldsymbol{\sigma}_{nr}$.

Governing equations in strong form of the introduced 2D models are written according to the two variational statements PVD and RMVT [4,16]. The first one, which states in the static case,

$$\int_V (\delta\boldsymbol{\epsilon}_{p_G}^{\mathrm{T}}\boldsymbol{\sigma}_{p_H} + \delta\boldsymbol{\epsilon}_{n_G}^{\mathrm{T}}\boldsymbol{\sigma}_{n_H})\,\mathrm{d}V = \delta L_e \tag{2}$$

is used to derive governing equations if only displacement assumptions are made. The superscript T signifies an array transposition while the subscript p denote in-plane components $\boldsymbol{\sigma}_p = \{\sigma_{xx}, \sigma_{yy}, \sigma_{xy}\}$, $\boldsymbol{\epsilon}_p = \{\epsilon_{xx}, \epsilon_{yy}, \epsilon_{xy}\}$. The subscript H denotes that stresses are computed via Hooke's law. The variation of the internal work has been split into in-plane and out-of-plane parts and involves stress from Hooke's law and strain from geometrical relations (subscript G). δL_e is the virtual variation of the work made by the external layer-force $\mathbf{p}$.

Reissner mixed variational theorem [26], which states,

$$\int_V (\delta\boldsymbol{\epsilon}_{p_G}^{\mathrm{T}}\boldsymbol{\sigma}_{p_H} + \delta\boldsymbol{\epsilon}_{n_G}^{\mathrm{T}}\boldsymbol{\sigma}_{n_M} + \delta\boldsymbol{\sigma}_{n_M}^{\mathrm{T}}(\boldsymbol{\epsilon}_{n_G} - \boldsymbol{\epsilon}_{n_H}))\,\mathrm{d}V = \delta L_e \tag{3}$$

is employed if both displacement and stress variables are assumed. The third 'mixed' term variationally enforces the compatibility of the transverse strain components. Subscript M denotes that transverse stresses are those of assumed model of Eq. (1).

2.1. Hooke's law and geometrical relation

The lamina are considered to be homogeneous and to operate in the linear elastic range. Stiffness coefficients are employed in standard form of the Hooke's law for the anisotropic k-lamina. This reads $\sigma_i = \widetilde{C}_{ij}\epsilon_j$ where the sub-indices i and j, ranging from 1 to 6, stand for the index couples 11, 22, 33, 13, 23 and 12, respectively. The material is assumed to be orthotropic as specified by: $\widetilde{C}_{14} = \widetilde{C}_{24} = \widetilde{C}_{34} = \widetilde{C}_{64} = \widetilde{C}_{15} = \widetilde{C}_{25} = \widetilde{C}_{35} = \widetilde{C}_{65} = 0$. This implies that σ_{xz}^k and σ_{yz}^k depend only on ϵ_{xz}^k and ϵ_{yz}^k. In matrix form,

$$\begin{aligned} \boldsymbol{\sigma}_{pH_d}^k &= \widetilde{\mathbf{C}}_{pp}^k\boldsymbol{\epsilon}_{pG}^k + \widetilde{\mathbf{C}}_{pn}^k\boldsymbol{\epsilon}_{nG}^k \\ \boldsymbol{\sigma}_{nH}^k &= \widetilde{\mathbf{C}}_{np}^k\boldsymbol{\epsilon}_{pG}^k + \widetilde{\mathbf{C}}_{nn}^k\boldsymbol{\epsilon}_{nG}^k \end{aligned} \tag{4}$$

where

$$\widetilde{\mathbf{C}}_{pp}^k = \begin{bmatrix} \widetilde{C}_{11}^k & \widetilde{C}_{12}^k & \widetilde{C}_{16}^k \\ \widetilde{C}_{12}^k & \widetilde{C}_{22}^k & \widetilde{C}_{26}^k \\ \widetilde{C}_{16}^k & \widetilde{C}_{26}^k & \widetilde{C}_{66}^k \end{bmatrix},$$

$$\widetilde{\mathbf{C}}_{pn}^k = \widetilde{\mathbf{C}}_{np}^{k\mathrm{T}} = \begin{bmatrix} 0 & 0 & \widetilde{C}_{13}^k \\ 0 & 0 & \widetilde{C}_{23}^k \\ 0 & 0 & \widetilde{C}_{36}^k \end{bmatrix}, \quad \widetilde{\mathbf{C}}_{nn}^k = \begin{bmatrix} \widetilde{C}_{44}^k & \widetilde{C}_{45}^k & 0 \\ \widetilde{C}_{45}^k & \widetilde{C}_{55}^k & 0 \\ 0 & 0 & \widetilde{C}_{66}^k \end{bmatrix}$$

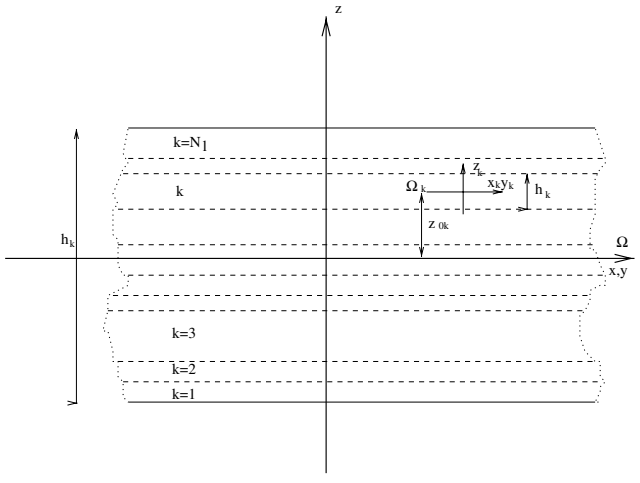

Fig. 1. Multilayered plate.

Bold letters denote arrays. The superscript T signifies array transposition. The subscripts n and p denote transverse (out-of-plane, normal) and in-plane values, respectively. Therefore

$$\boldsymbol{\sigma}_p^k = \{\sigma_{xx}^k, \sigma_{yy}^k, \sigma_{xy}^k\}, \quad \boldsymbol{\sigma}_n^k = \{\sigma_{xz}^k, \sigma_{yz}^k, \sigma_{zz}^k\}$$
$$\boldsymbol{\epsilon}_p^k = \{\epsilon_{xx}^k, \epsilon_{yy}^k, \epsilon_{xy}^k\}, \quad \boldsymbol{\epsilon}_n^k = \{\epsilon_{xz}^k, \epsilon_{yz}^k, \epsilon_{zz}^k\}$$

It should be noticed that σ_{zz} couples the in-plane and out-of-plane stress and strain components. Subscript H denotes stresses evaluated with Hooke's law while subscript G denotes the strain from the geometrical relation Eq. (6). Further subscript d signifies values employed in the displacement formulation. Eq. (4) is used in conjunction with a standard displacement formulation, while, for the adopted mixed solution procedure, the stress-strain relationships are conveniently put in the following mixed form,

$$\begin{aligned} \boldsymbol{\sigma}_{pH}^k &= \mathbf{C}_{pp}^k \boldsymbol{\epsilon}_{pG}^k + \mathbf{C}_{pn}^k \boldsymbol{\sigma}_{nM}^k \\ \boldsymbol{\epsilon}_{nH}^k &= \mathbf{C}_{np}^k \boldsymbol{\epsilon}_{pG}^k + \mathbf{C}_{nn}^k \boldsymbol{\sigma}_{nM}^k \end{aligned} \tag{5}$$

where both stiffness and compliance coefficients are employed. The subscript M states that the transverse stresses are those of the assumed model in Eq. (1). The relation between the arrays of coefficients in the two forms of Hooke's law is simply found

$$\mathbf{C}_{pp}^k = \widetilde{\mathbf{C}}_{pp}^k - \widetilde{\mathbf{C}}_{pn}^k \widetilde{\mathbf{C}}_{nn}^{k^{-1}} \widetilde{\mathbf{C}}_{np}^k, \quad \mathbf{C}_{pn}^k = \widetilde{\mathbf{C}}_{pn}^k \widetilde{\mathbf{C}}_{nn}^{k^{-1}}$$
$$\mathbf{C}_{np}^k = -\widetilde{\mathbf{C}}_{nn}^{k^{-1}} \widetilde{\mathbf{C}}_{np}^k, \quad \mathbf{C}_{nn}^k = \widetilde{\mathbf{C}}_{nn}^{k^{-1}}$$

Superscript -1 denotes an inversion of the array.

The strain components $\boldsymbol{\epsilon}_p^k$, $\boldsymbol{\epsilon}_n^k$ are linearly related to the displacements $\mathbf{u}^k$ $(\{u_x^k, u_y^k, u_z^k\})$, according to the following geometrical relations:

$$\boldsymbol{\epsilon}_{pG}^k = \mathbf{D}_p \mathbf{u}^k, \quad \boldsymbol{\epsilon}_{nG}^k = \mathbf{D}_n \mathbf{u}^k \tag{6}$$

$\mathbf{D}_p$ and $\mathbf{D}_n$ denotes in-plane and out-of-plane differential operators

$$\mathbf{D}_p = \begin{bmatrix} \partial_x & 0 & 0 \\ 0 & \partial_y & 0 \\ \partial_y & \partial_x & 0 \end{bmatrix}; \quad \mathbf{D}_n = \begin{bmatrix} \partial_z & 0 & \partial_x \\ 0 & \partial_z & \partial_y \\ 0 & 0 & \partial_z \end{bmatrix}$$

3. Implemented theories

The thickness assumptions that were used in Eqs. (1) permit one to develop a large variety of two-dimensional theories. Depending on the variational statement used (PVD or RMVT), the description of the variables (LWM or ESLM), the order of the expansion used N, a number of two-dimensional theories can be constructed. Such a variety of sandwich theories fits very well with the assessment proposed in this paper. In fact, these theories are able to cover a large part of the known classical and refined modelings of multilayered plates. The richest one, such as LM4, leads to a quasi three-dimensional description of layered plates; the poorest, such as ED1, leads to results very close to CLT and FSDT type approximations. A few details on the assumptions related to selected plate theories that have been used in this work is given below. Fig. 2 shows the manners in which acronyms have been built. Details can be read in the already mentioned authors' works.

3.1. Plate theories with only displacement variables

3.1.1. ESLM classical models: ED1, ED1d, ED4

The Taylor type expansion is used for the displacements in the plate thickness direction. Subscript b denotes values with correspondence to Ω $(\mathbf{u}_b = \mathbf{u}_0)$; subscript t refers to the highest order term $(\mathbf{u}_t = \mathbf{u}_N)$; subscript r refers to the higher order terms. The F_τ polynomials assume the following explicit form

$$F_b = 1, \quad F_r = z^r, \quad F_t = z$$

ED1 theories refer to $N = 1$ expansion. In case of ED1d the F_t term is removed from the expansion of transverse displacements u_z. That is, the last letter 'd' of the acronym denotes that transverse normal strain is not accounted for. In the ED4 case the Taylor expansion is truncated to the forth order term $N = 4$. ED1d and ED4 analyses consist of the poorest and the richest possibilities in the framework of classical ESL theories for laminated plates.

3.2. Theories with displacement and transverse stress variables

3.2.1. ESLM cases: EMZC3, EMZC3d

It is possible to introduce ZZ effects in the previous expansion for displacement by referring to Murakami zig-zag function, which was originally introduced in the framework of RMVT. Murakami [27] proposed to add a zig-zag type function in a Taylor type expansion. According to our notations, one can assume

$$F_t = (-1)^k \zeta_k$$

where $\zeta_k = 2z_k/h_k$ is a non-dimensional layer coordinate, z_k is the physical coordinate of the k-layer of thickness h_k. The exponent k changes the sign of the ZZ term in each layer. Such an zig-zag function permits one to reproduce the discontinuity of the first derivative of the displacement variables in the z-directions which physically comes from the intrinsic transverse anisot-

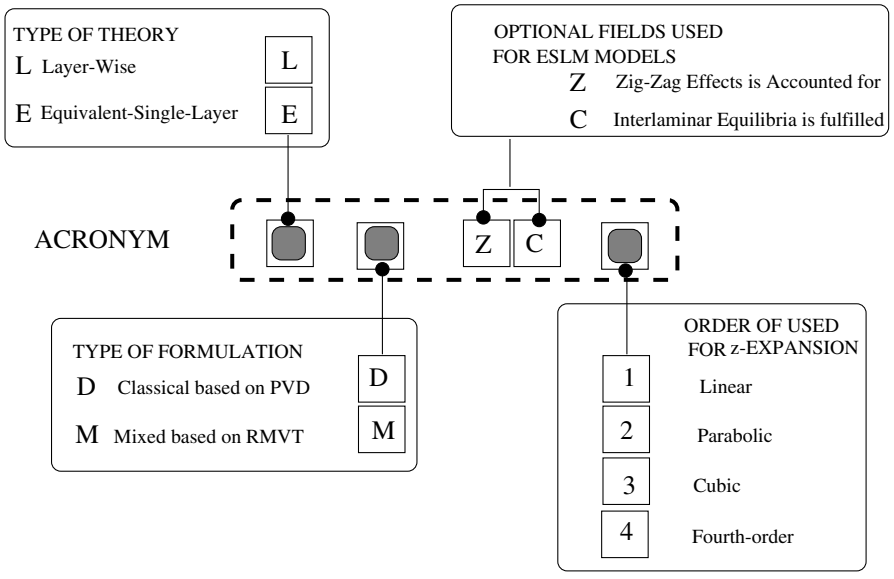

Fig. 2. Meanings of the introduced acronyms.

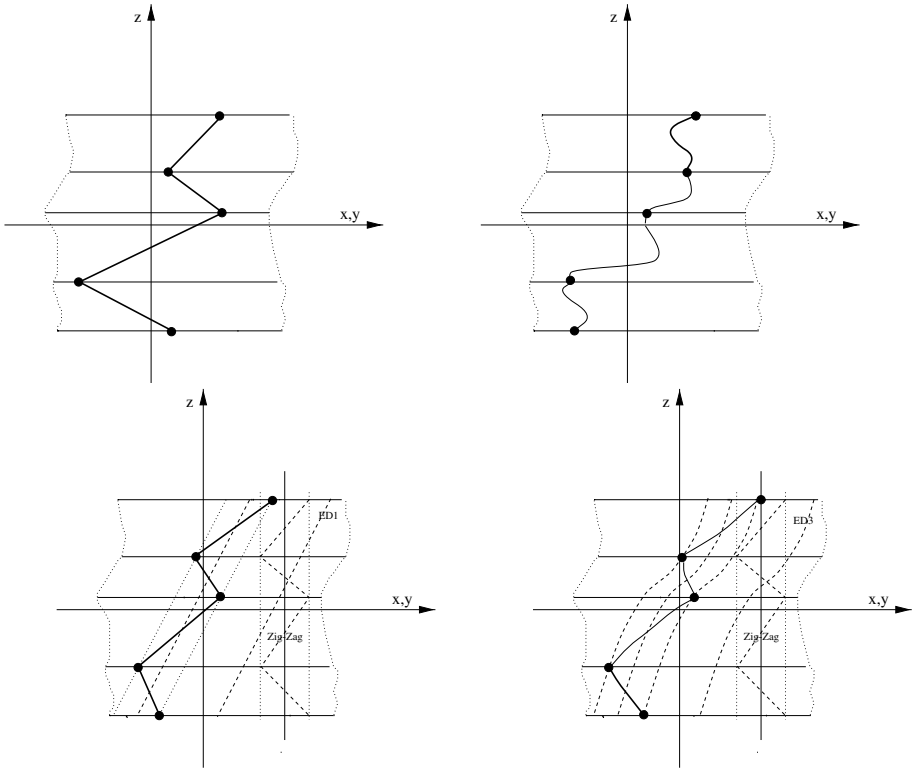

Fig. 3. Examples of trough-the-thickness fields. LWM (upper part, linear and higher order cases) and ESLM (including Murakami zig-zag function) assumptions in a four layered plate.

ropy of multilayered made structures (see Fig. 3, lower part).

Taylor-type expansion is not appropriate for ESL description of transverse stresses. Its use would require additional constrains in order to fulfill transverse shear and normals stress continuity. The use of RMVT demands layers wise description of transverse stresses even though ESLM expansions are used for displacements. A convenient layer-wise description is simply obtained by referring to a combination of Legendre polynomials. The subscripts t and b denote values related to the layer top and bottom surface, respectively. These two terms consist of the linear part of the expansion. The thickness functions $F_\tau(\zeta_k)$ have now been defined at the k-layer level,

$$F_t = \frac{P_0 + P_1}{2}, \quad F_b = \frac{P_0 - P_1}{2}, \quad F_r = P_r - P_{r-2}, \quad r = 2, 3, \ldots, N$$

in which $P_j = P_j(\zeta_k)$ is the Legendre polynomial of the j-order defined in the ζ_k-domain: $-1 \leqslant \zeta_k \leqslant 1$.

The plate theories referred to as EMZC3 uses a third order Taylor- type displacement models in addition to the Murakami function. Four order Legendre expansion is instead used for transverse stresses. EMZC3d is a particular cases of EMZC3 in which transverse normal strains are neglected. That is done by removing linear to forth order terms in the z-expansion of u_z.

Already mentioned first author's works have been shown that EMZC3 analyses consists on the best available refined theory in the ESL framework.

3.2.2. LW cases: LM2, LM4

A layer-wise description is simply obtained by extending the stress assumption of previous point (1) to displacement variables. LM2 and LM4 refer to parabolic and to forth order expansions in each layer for both displacements and transverse stresses, respectively. Already mentioned first author's works have been shown that LM4 analyses leads to quasi 3D description of the response of laminated plates.

4. Governing equations

Upon substitution of introduced displacement and stress models, as well as a suitable geometric relation and Hooke's law, and by integrating by parts, the two described variational equations, PVD and RMVT, lead to governing differential equations in terms of the introduced stress and displacement variables. The displacement formulation yields to the following equilibrium conditions

$$\delta \mathbf{u}_\tau^k: \quad \mathbf{K}_d^{k\tau s}\mathbf{u}_s^k = \mathbf{p}_\tau^k \tag{7}$$

the related boundary conditions are

$$\mathbf{u}_\tau^k = \bar{\mathbf{u}}_\tau^k \quad \text{or} \quad \mathbf{\Pi}_d^{k\tau s}\mathbf{u}_s^k = \mathbf{\Pi}_d^{k\tau s}\bar{\mathbf{u}}_s^k \tag{8}$$

The mixed case leads to the following set of equilibrium and constitutive equations

$$\begin{aligned} &\delta \mathbf{u}_\tau^k: \quad \mathbf{K}_{uu}^{k\tau s}\mathbf{u}_s^k + \mathbf{K}_{u\sigma}^{k\tau s}\boldsymbol{\sigma}_{ns}^k = \mathbf{p}_\tau^k \\ &\delta \boldsymbol{\sigma}_{n\tau}^k: \quad \mathbf{K}_{\sigma u}^{k\tau s}\mathbf{u}_s^k + \mathbf{K}_{\sigma\sigma}^{k\tau s}\boldsymbol{\sigma}_{ns}^k = 0 \end{aligned} \tag{9}$$

and to the boundary conditions

$$\mathbf{u}_\tau^k = \bar{\mathbf{u}}_\tau^k \quad \text{or} \quad \mathbf{\Pi}_u^{k\tau s}\mathbf{u}_s^k + \mathbf{\Pi}_\sigma^{k\tau s}\boldsymbol{\sigma}_{ns}^k = \mathbf{\Pi}_u^{k\tau s}\bar{\mathbf{u}}_s^k + \mathbf{\Pi}_\sigma^{k\tau s}\bar{\boldsymbol{\sigma}}_{ns}^k \tag{10}$$

The further subscript/superscript $s = t,\ b,\ r$ has been introduced in order to distinguish the terms related to the introduced variables from those related to their variations.

In explicit form

$$\begin{aligned} \mathbf{K}_d^{k\tau s} &= -\mathbf{D}_p^{\mathrm{T}}(\tilde{\mathbf{Z}}_{pp}^{k\tau s}\mathbf{D}_p + \tilde{\mathbf{Z}}_{pn}^{k\tau s}\mathbf{D}_{n\Omega} + \tilde{\mathbf{Z}}_{pn}^{k\tau s_z}\mathbf{D}_{n\Omega}) \\ &\quad - \mathbf{D}_{n\Omega}^{\mathrm{T}}(\widetilde{\mathbf{Z}}_{np}^{k\tau s}\mathbf{D}_p + \widetilde{\mathbf{Z}}_{nn}^{k\tau s}\mathbf{D}_{n\Omega} + \widetilde{\mathbf{Z}}_{nn}^{k\tau s_z}) \\ &\quad + \tilde{\mathbf{Z}}_{np}^{k\tau_z s}\mathbf{D}_p + \tilde{\mathbf{Z}}_{nn}^{k\tau_z s}\mathbf{D}_{n\Omega} + \widetilde{\mathbf{Z}}_{nn}^{k\tau_z s_z} \\ \mathbf{\Pi}_d^{k\tau s} &= \mathbf{I}_p^{\mathrm{T}}(\widetilde{\mathbf{Z}}_{pp}^{k\tau s}\mathbf{D}_p + \widetilde{\mathbf{Z}}_{pn}^{k\tau s}\mathbf{D}_{n\Omega} + \widetilde{\mathbf{Z}}_{pn}^{k\tau s_z}\mathbf{D}_{n\Omega}) \\ &\quad + \mathbf{I}_{n\Omega}^{\mathrm{T}}(\tilde{\mathbf{Z}}_{np}^{k\tau s}\mathbf{D}_p + \widetilde{\mathbf{Z}}_{nn}^{k\tau s}\mathbf{D}_{n\Omega} + \widetilde{\mathbf{Z}}_{nn}^{k\tau s_z}) \\ \mathbf{K}_{uu}^{k\tau s} &= -\mathbf{D}_p^{\mathrm{T}}\mathbf{Z}_{pp}^{k\tau s}\mathbf{D}_p \quad \mathbf{K}_{u\sigma}^{k\tau s} = -\mathbf{D}_p^{\mathrm{T}}\mathbf{Z}_{pn}^{k\tau s} + E_{\tau_z s}\mathbf{I} - E_{\tau s}\mathbf{D}_{n\Omega}^{\mathrm{T}} \\ \mathbf{K}_{\sigma u}^{k\tau s} &= E_{\tau s}\mathbf{D}_{n\Omega} + E_{\tau s_z}\mathbf{I} - \mathbf{Z}_{np}^{k\tau s}\mathbf{D}_p \quad \mathbf{K}_{\sigma\sigma}^{k\tau s} = -\mathbf{Z}_{nn}^{k\tau s} \\ \mathbf{\Pi}_u^{k\tau s} &= \mathbf{I}_p^{\mathrm{T}}\mathbf{Z}_{pp}^{k\tau s}\mathbf{D}_p \quad \mathbf{\Pi}_\sigma^{k\tau s} = \mathbf{Z}_{pn}^{k\tau s} + E_{\tau s}\mathbf{I}_{n\Omega}^{\mathrm{T}} \end{aligned} \tag{11}$$

where

$$\mathbf{D}_{n\Omega} = \begin{bmatrix} 0 & 0 & \partial_x \\ 0 & 0 & \partial_y \\ 0 & 0 & 0 \end{bmatrix}; \quad \mathbf{I} = \begin{bmatrix} 1 & 0 & 0 \\ 0 & 1 & 0 \\ 0 & 0 & 1 \end{bmatrix};$$

$$\mathbf{I}_p = \begin{bmatrix} 1 & 0 & 0 \\ 0 & 1 & 0 \\ 1 & 1 & 0 \end{bmatrix}; \quad \mathbf{I}_{n\Omega} = \begin{bmatrix} 0 & 0 & 1 \\ 0 & 0 & 1 \\ 0 & 0 & 0 \end{bmatrix}$$

The integration in the thickness coordinate has been a priori carried out as usual in two-dimensional modelings: the following layer-stiffnesses and integrals have been introduced

$$\begin{aligned} &(\widetilde{\mathbf{Z}}_{pp}^{k\tau s}, \widetilde{\mathbf{Z}}_{pn}^{k\tau s}, \widetilde{\mathbf{Z}}_{np}^{k\tau s}, \widetilde{\mathbf{Z}}_{nn}^{k\tau s}, \mathbf{Z}_{pp}^{k\tau s}, \mathbf{Z}_{pn}^{k\tau s}, \mathbf{Z}_{np}^{k\tau s}, \mathbf{Z}_{nn}^{k\tau s}) \\ &\quad = (\widetilde{\mathbf{C}}_{pp}^k, \widetilde{\mathbf{C}}_{pn}^k, \widetilde{\mathbf{C}}_{np}^k, \widetilde{\mathbf{C}}_{nn}^k, \mathbf{C}_{pp}^k, \mathbf{C}_{pn}^k, \mathbf{C}_{np}^k, \mathbf{C}_{nn}^k)E_{\tau s} \\ &(\widetilde{\mathbf{Z}}_{pn}^{k\tau s_z}, \widetilde{\mathbf{Z}}_{np}^{k\tau_z s}, \widetilde{\mathbf{Z}}_{nn}^{k\tau s_z}, \widetilde{\mathbf{Z}}_{nn}^{k\tau_z s}, \widetilde{\mathbf{Z}}_{nn}^{k\tau_z s_z}) \\ &\quad = (\widetilde{\mathbf{C}}_{pn}^k E_{\tau s_z}, \widetilde{\mathbf{C}}_{np}^k E_{\tau_z s}, \widetilde{\mathbf{C}}_{nn}^k E_{\tau s_z}, \widetilde{\mathbf{C}}_{nn}^k E_{\tau_z s}, \widetilde{\mathbf{C}}_{nn}^k E_{\tau_z s_z}) \\ &(E_{\tau s}^k, E_{\tau_z s}, E_{\tau s_z}, E_{\tau_z s_z}^k) = \int_{A_k} (F_\tau F_s, F_{\tau_z} F_s, F_\tau F_{s_z}, F_{\tau_z} F_{s_z})\,\mathrm{d}z \end{aligned} \tag{12}$$

Explicit forms of the governing equations for each layer can be written by expanding the introduced subscripts and superscripts in the previous arrays as follows

$k = 1, 2, \ldots, N_l; \quad \tau = t, r, b, \quad s = t, r, b,$
$(r = 2, \ldots, N)$

4.1. Closed form solutions

The obtained boundary values problem governed in the most general case of geometry, boundary conditions and lay-outs, could be solved by implementing only approximated solution procedures. In the particular case in which the material has orthotropic behavior, Navier-type closed form solutions can be found by assuming the harmonic forms for the applied loadings and unknown variables:

$$\begin{aligned}
(u^k_{x_\tau}, \sigma^k_{xz_\tau}, p^k_{x_\tau}) &= \sum_{m,n} (U^k_x, S^k_{xz_\tau}, P^k_{x_\tau}) \cos\frac{m\pi x}{a} \sin\frac{n\pi y}{b} \\
(u^k_{y_\tau}, \sigma^k_{yz_\tau}, p^k_{y_\tau}) &= \sum_{m,n} (U^k_y, S^k_{yz_\tau}, P^k_{y_\tau}) \sin\frac{m\pi x}{a} \cos\frac{n\pi y}{b} \\
(u^k_{z_\tau}, \sigma^k_{zz_\tau}, p^k_{z_\tau}) &= \sum_{m,n} (U^k_z, S^k_{zz_\tau}, P^k_{z_\tau}) \sin\frac{m\pi x}{a} \sin\frac{n\pi y}{b}
\end{aligned} \tag{13}$$

while m and n are the correspondent wave numbers. Capital letters in the R.H.S. are correspondent maximum amplitudes. On substitution of Eq. (13), the governing equations assume the form of a linear system of algebraic equations. This procedure has been coded for the different case theories and results are discussed in the next sections.

Navier-type solution can be extended to any type of applied loading unless an appropriate Fourier expansions is made. The benchmarks described in the next sections are related to transverse distribution of constant pressure p_{zT} and to point lading P_z cases. The appropriate Fourier expansion to these two cases should be written as,

$$(p_{zT}, P_z) = \sum_{m,n}^{R,Q} (p^{mn}_{zT}, P^{mn}_{zT}) \sin\frac{m\pi x}{a} \sin\frac{n\pi y}{b} \tag{14}$$

where R, Q are the maximum values of the considered m and n, while p^{mn}_{zT}, P^{mn}_{zT} are the coefficients of the Fourier series.

The systems of algebraic equations that come upon substation of Navier type solutions in Eqs. (7)–(10), have not been explicitly quoted.

5. Benchmarks description

In order to investigate the accuracy of plate theories vs their response to localized loadings, four benchmark problems have been considered as desk beds to assess two-dimensional theories. These have been depicted in Fig. 4 and detailed in the next paragraphs.

5.1. BM1: sandwich plate loaded by uniform distribution of transverse pressure

This is a moderately thick, unsymmetrically laminated, rectangular sandwich plate loaded by a uniform distribution p_{zT} of transverse pressure applied to the whole top surface Ω_{BM1}. The plate is simply supported with correspondence to their four edges. The plate geometrical parameters hold: $a = 100$ mm, $b = 200$ mm, $h = 12$ mm. The loaded area is therefore,

$$\Omega_{BM1} = 100 \times 200 \ [\text{mm}^2]$$

The faces, of same material, have different thicknesses: top face thickness $h_3 = 0.1$ mm, bottom face thickness $h_1 = 0.5$ mm. The core thickness is $h_1 = 11.4$ [mm]. The two faces have the following material datas:

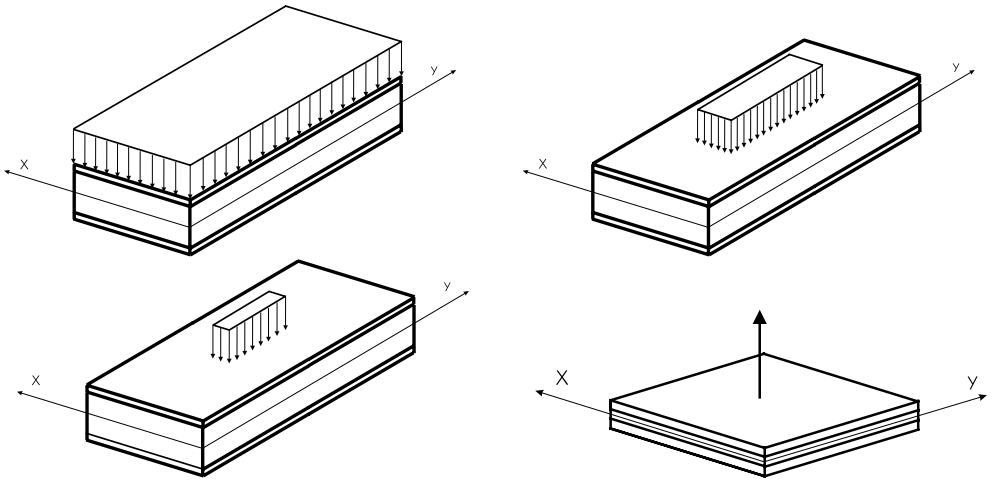

Fig. 4. The four considered benchmarks BM1 (left-top), BM2 (right-top), BM3 (left-bottom), BM4 (right-bottom).

$E_x = 70,000$ MPa, $E_y = 71,000$ MPa,
$E_z = 69,000$ MPa

$E_{xz} = 26,000$ MPa, $E_{yz} = 26,000$ MPa,
$E_{yz} = 26,000$ MPa $v_{xz} = v_{yz} = v_{yz} = 0.3$

The core consists of metallic foam which has the following mechanical datas

$E_x = E_y = 3$ MPa, $E_z = 2.8$ MPa,
$E_{xz} = E_{yz} = E_{yz} = 1$ MPa $v_{xz} = v_{yz} = v_{yz} = 0.25$

BM1 has been originated by modifying the benchmark problem originally proposed by Meyer-Piening [22], see BM3.

5.2. BM2: sandwich plate loaded by localized distribution of transverse pressure over Ω_{BM2}

BM2 coincides with BM1 with exception made for the loaded surface which is now located at the plate center over the area

$\Omega_{\mathrm{BM2}} = 20 \times 80$ [mm^2]

5.3. BM3: sandwich plate loaded by localized distribution of transverse pressure over Ω_{BM3}

BM3 coincides with BM1 exception made for the loaded surface which is now located at the plate center over the area

$\Omega_{\mathrm{BM2}} = 5 \times 20$ [mm^2]

BM3 coincides with problem proposed by Meyer-Piening [22] who provided a 3D analytical solutions as well as FEM analyses (conducted by means of commercial code Nastran, 3D brick elements were used for the core and plate elements for the two faces). It was also used in [25] to assess the finite elements proposed in [28].

p_{zT} should be reduced in the BM1 and BM2 analyses in order to avoid high stress values. That has not been done in the present work. However, being the problem linear, high stress values could be lowered by reducing p_{zT} in the requested cases.

5.4. BM4: cross-ply plate subjected to point load

BM4 consists of a square, symmetrically laminated cross-ply plate bent by a point load P_z located at the plate center. The plate consists of three layers of equal thickness $h_1 = h_2 = h_3 = h/3$ with stacking sequence 0°/90°/0°. The mechanical properties of the laminae which are:

$E_L/E_T = 25$, $G_{\mathrm{LT}}/E_T = 0.5$, $G_{\mathrm{TT}}/E_T = 0.2$,
$v_{\mathrm{LT}} = v_{\mathrm{TT}} = 0.25$

where following usual notations [3], L signifies the fiber direction, T the transverse direction and v_{LT} is the major Poisson ratio.

6. Numerical analyses

A number of numerical simulations have conducted for BM1–BM4. In-plane and out-of-plane stresses and displacements were determined for several plate theories. The most significant results are discussed in the next subsections in the form of tables and diagrams.

6.1. BM1 results

The stresses and displacements were expressed in the following form:

$$\overline{U}_z = U_z \frac{\Omega_{\mathrm{BM3}}}{\Omega_{\mathrm{BM1}}}, \quad (\overline{S}_{xx}, \overline{S}_{yy}) = \frac{(S_{xx}, S_{xx})}{p_{zT}}$$

These representation will be also used for BM2 and BM3 analyses, in which Ω_{BM1} will be replaced by Ω_{BM2} and by Ω_{BM1}, respectively. The number of the terms of the Fourier expansion for the applied loading was fixed at $R = Q = 25$ for BM1–BM2–BM3. The averaged errors were indicated. These were determined as,

$$\text{Err-3D} = \left| \frac{V_{\mathrm{CT}} - V_{\mathrm{3D}}}{V_{\mathrm{3D}}} \right|, \quad \text{Err-LM4} = \left| \frac{V_{\mathrm{CT}} - V_{\mathrm{LM4}}}{V_{\mathrm{LM4}}} \right|$$

where V_{CT} denotes the values of the actual theory while V_{3D} and V_{LM4} denote the values that correspond to 3D and LM4 analyses, respectively.

The BM1 results are presented in Tables 1 and 2 and Figs. 5 and 6. The transverse displacements of the top and bottom surfaces of the sandwich panels are

Table 1
BM1: transverse displacements $\overline{U}_z$ ($R = Q = 25$)

	Top face	Err-LM4 (%)	Bottom face	Err-LM4 (%)
LM4	−0.4571	–	−0.4484	–
EMZC3	−0.3682	19.45	−0.3649	18.62
EMZC3d	−0.3633	20.52	−0.3633	18.98
ED1	−0.005111	98.88	−0.005098	0.9886
ED1d	−0.005100	98.89	−0.005100	0.9886

Table 2
BM1: in-plane stresses $\overline{S}_{xx}$ and $\overline{S}_{yy}$ ($R = Q = 25$)

	z	Top face			Bottom face		
		$\overline{S}_{xx}$	Err-LM4 (%)	$\overline{S}_{yy}$	$\overline{S}_{xx}$	Err-LM4 (%)	$\overline{S}_{yy}$
LM4	Top	−1124.0	–	−528.24	−1332.1	–	−543.27
	Bot	−484.35	–	−233.20	1662.7	–	699.15
EMZC3	Top	−1183.1	0.5256	−625.24	−1193.1	10.43	−575.54
	Bot	−396.78	18.08	−114.3	1518.0	8.702	714.29
EMZC3d	Top	−1118.0	0.5338	−633.29	−1331.9	0.0015	−698.42
	Bot	−518.05	6.958	−315.25	1663.5	0.0048	889.44
ED1	Top	−896.30	20.25	−514.53	155.08	88.35	84.375
	Bot	−887.15	83.16	−509.32	200.08	87.96	110.41
ED1d	Top	−895.69	20.31	−510.23	155.68	88.31	88.672
	Bot	−886.55	83.04	−505.02	201.4	87.88	114.31

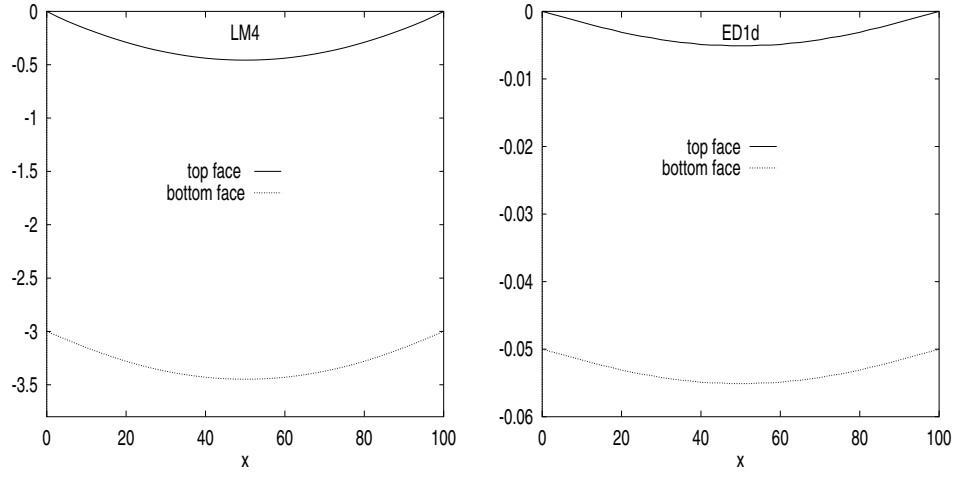

Fig. 5. BM1: trough-the-width distribution of transverse displacements $\overline{U}_z$ of top and bottom faces ($R = Q = 25$). Comparison between LM4 and ED1d analyses.

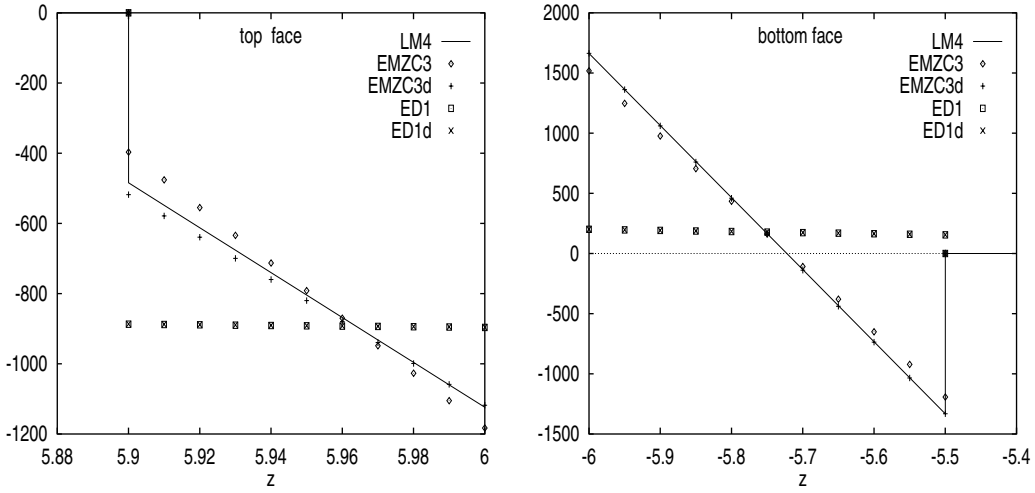

Fig. 6. BM1: in-plane stresses distribution $\overline{S}_{xx}$ in the two sandwich faces. Comparison among five significant theories.

compared in Table 1. Five significant theories were compared. LM4 was taken as the reference solutions wherever 3*D* analysis was not available. Even though the plate is moderately thick ($a/h = 10$ and $b/h = 20$) and a uniform distribution of transverse pressure is applied, one can notice that the classical theories (discarding ED1d and including normal strain deformation), totally fail to predict U_z. The quality of the solution of LM4 and ED1d is the same, as shown by Fig. 5. Refined theories (EMZC3) that include IC and ZZ effects lead to significant errors (about twenty percent). In-plane stress distributions in the two faces was addressed, as can be seen in Table 2 and Fig. 5. The discrepancies found in Table 1 are confirmed by Table 2 results which give local values of stresses. Fig. 5 shows that the in-plane stress distributions in the sandwich faces are very steep. A minor error in predicting their slope could lead to very large error for the local distribution of stresses related to ESLM analyses. Errors related to the top and bottom values can, in fact, be very different. ED1 and ED1d theories are ineffective in capturing the different behavior exhibited by the top and bottom sandwich faces.

6.2. BM2 results

The results related to BM2 analyses are reported in Tables 3 and 4 and Figs. 7 and 8. Fig. 7 shows that different theories lead to very different capabilities to trace, even from a qualitative point of view, the response of the top, loaded surface: the localized loading produces a local bending of the top surface which is captured by LM4 and EMZC3 analyses but not by EMZC3d, nor by the ED1 ones. EMZC3d analyses, that neglect transverse normal strain, are, in fact, ineffective in capturing the core transverse normal deformations: the related top and bottom surface deformations therefore appear similar in Fig. 7. ED1 analyses, which includes transverse normal strain, leads to very large error, that is, LWM analysis is required to accurately predict the behavior of the loaded faces. This is confirmed by the number quoted in Table 3 which shows larger errors compared to Table 1 analyses: ESLM results related to the BM2 problem are less accurate than those already obtained by BM1 analyses. The trend is confirmed by the stress analyses that are reported in Table 4 and Fig. 8. The very steep forms of the in-plane distributions of stresses in the sandwich faces should be noticed once again.

6.3. BM3 results

BM3 coincides with the original problem which was first considered by Meyer-Piening in [22]. The results are quoted in Tables 5 and 6 and Figs. 9–12. The available closed form solutions, as well as the FEM results provided in [22,25] are given for comparison purposes in Tables 5–7. These comparisons prove the effectiveness of the present LW analyses. The top-bottom surface deformations related to the LM2 analyses have been plotted in Fig. 9. This figure clearly shows the localized

Table 3
BM2: transverse displacements $\overline{U}_z$ $(R = Q = 25)$

	Top face	Err-LM4 (%)	Bottom face	Err-LM4 (%)
LM4	−1.6174	–	−1.4633	–
EMZC3	−1.2745	21.20	−1.1912	18.59
EMZC3d	−1.2030	25.62	−1.2030	17.79
ED1	−0.01391	99.13	−0.01375	99.06
ED1d	−0.01378	99.15	−0.01378	99.06

Table 4
BM2: in-plane stresses $\overline{S}_{xx}$ and $\overline{S}_{yy}$ $(R = Q = 25)$

	z	Top face			Bottom face		
		$\overline{S}_{xx}$	Err-LM4 (%)	$\overline{S}_{yy}$	$\overline{S}_{xx}$	Err-LM4 (%)	$\overline{S}_{yy}$
LM4	Top	−430.63	–	−245.43	−665.29	–	−334.61
	Bot	33.72	–	14.37	927.06	–	473.15
EMZC3	Top	−473.07	8.971	−319.37	−833.29	25.25	−505.24
	Bot	107.76	219.6	111.51	911.05	1.723	536.66
EMZC3d	Top	−395.53	16.29	−21.14	−944.3	41.93	−557.04
	Bot	−0.39027	98.83	−16.76	1027.1	10.79	612.4
ED1	Top	−248.89	47.38	−167.32	43.474	93.46	25.02
	Bot	−246.37	630.6	−165.66	55.14	94.05	32.51
ED1d	Top	−248.23	47.53	−163.15	43.14	93.52	28.36
	Bot	−245.95	629.4	−161.65	55.81	93.98	36.68

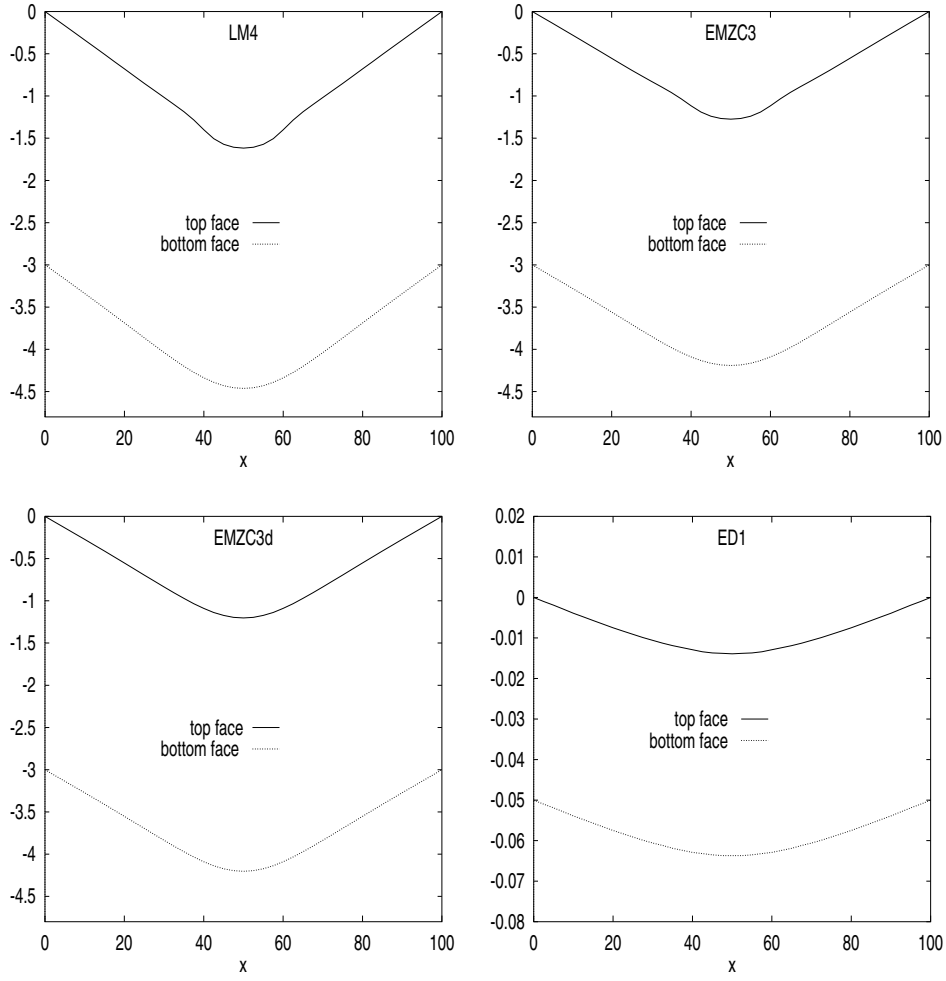

Fig. 7. BM2: trough-the-width distribution of transverse displacements $\overline{U}_z$ of top and bottom faces ($R = Q = 25$). Comparison among four significant theories.

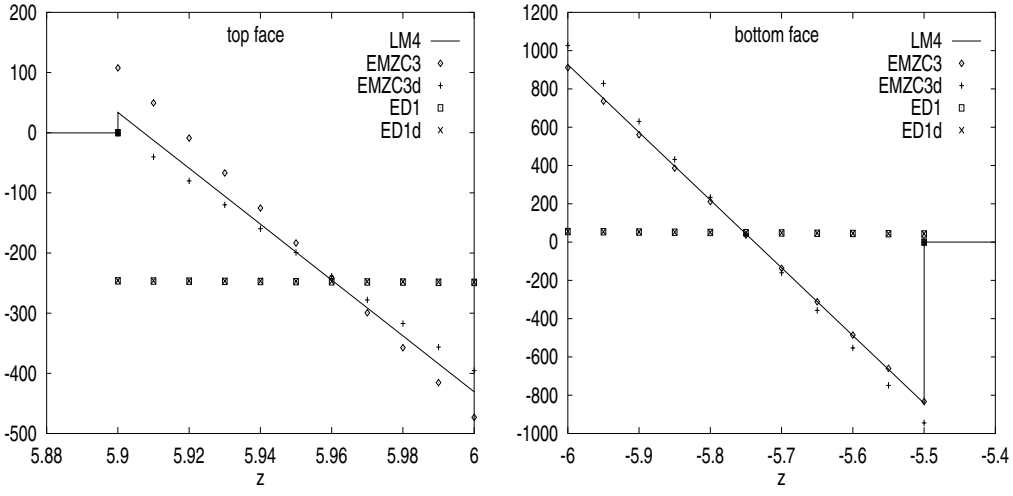

Fig. 8. BM2: in-plane stresses distribution $\overline{S}_{xx}$ in the two sandwich faces. Comparison among five significant theories ($R = Q = 25$).

bending of the top surface. The Fig. 7 comments are confirmed. The errors increase with respect to the displacement and the the stress analyses related to the BM1 and BM2 numerical evaluations. It is of interest to

Table 5
BM3: transverse displacements $\overline{U}_z$

	Top face	Err-3D	Err-3D (%)	Bottom face (%)
3D [22]	−3.78	–	−2.14	–
Present analyses ($R = Q = 25$)				
LM2	−3.8243	1.171	−2.1412	0.0
EMZC3	−2.8026	25.86	−1.7249	19.40
EMZC3d	−1.8599	50.80	−1.8599	13.09
ED1	−0.019175	99.49	−0.017496	99.18
ED1d	−0.017804	99.53	−0.017804	99.17
FEM analyses				
NASTRAN 3D [22]	−3.84	1.587	−2.19	2.336
LM2 [25]	−3.7628	0.4550	−2.19	2.336
EMZC3 [25]	−2.0483	45.85	−1.8717	12.53
ED1 [25]	−0.0187	99.51	−0.0181	99.16

Table 6
BM3: in-plane stress $\overline{S}_{xx}$

	z	Top face	Err-3D (%)	Bottom face	Err-3D (%)
3D [22]	Top	−624	–	−138	–
	Bot	580	–	146	–
Present analyses ($R = Q = 25$)					
LM2	Top	−619.49	0.7227	−138.11	0.0
	Bot	577.36	0.4551	145.88	0.0822
EMZC3	Top	−486.07	22.10	−233.34	69.08
	Bot	455.55	21.45	220.58	51.08
EMZC3d	Top	−69.749	88.88	−261.93	89.80
	Bot	37.689	93.50	270.85	85.51
ED1	Top	−30.02	95.19	4.38	96.82
	Bot	−29.722	94.87	5.72	96.08
ED1d	Top	−29.179	95.29	5.0715	96.36
	Bot	−28.881	95.02	6.5606	0.9550
FEM analyses					
NASTRAN 3D [22]	Top	−628	0.6410	−140	1.449
	Bot	582	0.3448	148	1.369
LM2 [25]	Top	−595.56	0.4557	−136.2	1.304
	Bot	556.23	0.3448	144.03	1.369
ED1 [25]	Top	−29.46	95.27	4.87	96.47
	Bot	−29.17	94.97	6.36	95.64

notice the increasing role played by transverse strain deformation: the inclusion of transverse normal strains in ED1 analyses barely shows the localized bending region of the top face. This is not captured by EMZC3d, which gives much better results than ED1 due to capability of EMZC3 to include IC and ZZ effects. The transverse strain effect is detailed in Fig. 10, which plots of the transverse displacement distribution in the sandwich plate thickness. The 3D plots of top and bottom surface deformations for the LM2 and EMZC3 theories are given in Fig. 12.

6.4. BM4 results

Results related to point load $P_z = P$ plates are given in Tables 7 and 8 and Figs. 13–18. The displacements and stresses were calculated according to the following formulas,

$$U_z' = \frac{U_z 100 E_T h^3}{P_z a^2}, \quad (S_{xx}', S_{yy}', S_{xy}', S_{xz}', S_{yx}', S_{zz}') = \frac{1}{P_z}(S_{xx}, S_{yy}, S_{xy}, S_{xz}, S_{yx}, S_{zz})$$

The implicit singularity that is included in the point loading case requires higher order Fourier expansion compared to BM1–BM3 analyses. Tables 7 and 8 show that: U_z' and S_{xx}' have higher convergence rate with respect in-plane and transverse stress evaluations, respectively; the plate thickness ratio influences displacement and stress evaluations in a different manner; required order R, Q for the convergent solution is also influenced by plate theories and plate geometries. Further hints on

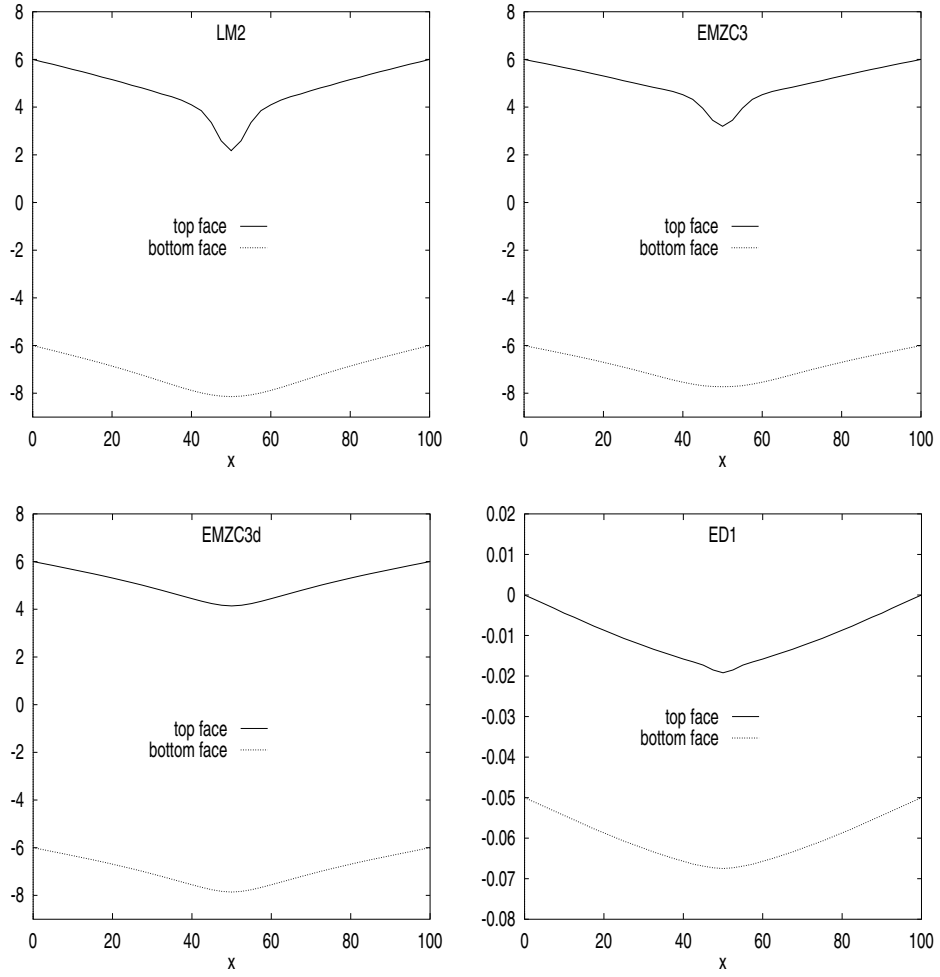

Fig. 9. BM3: trough-the-width distribution of transverse displacements $\overline{U}_z$ of top and bottom faces ($R = Q = 25$). Comparison among four significant theories.

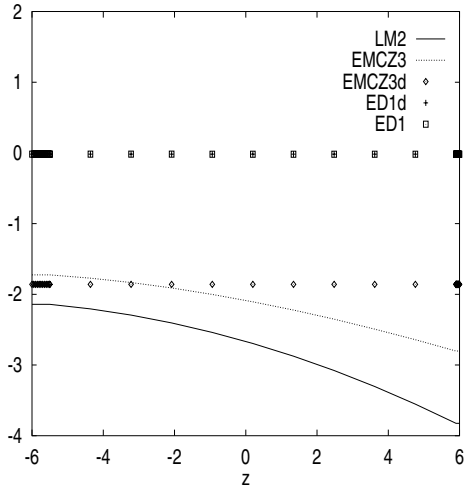

Fig. 10. BM3: trough-the-thickness distribution of $\overline{U}_z$ ($R = Q = 25$). Comparison among five significant theories.

the R, Q effects of through the thickness distribution of displacement and stresses related to LM4 analyses are given in Figs. 13–15. Fig. 13, in the thick plate case (left part), shows that by increasing R and Q, the transverse displacement leads to the expected singularities $U_z = \infty$ with correspondence to the point in which P_z was applied. In other words, the presented LM4 analysis is very effective in tracing the response of a plate subject to point loadings. On the other hand, the thin plate (right part) shows a slow convergence rate to the expected singularity. Numerical simulations, that have not been completely documented herein, have shown that the Fourier series could diverge by further increasing of the R, Q values. Fig. 14 confirms the previous comments for in-plane stress evaluations. The singularity $S'_{xx} = \infty$ is very rapidly approached in thick plate cases. Some oscillations must be registered by R, Q increasing. Fig. 15 confirms the trend of Figs. 13 and 14 for transverse stress evaluations. The difficulties of the Fourier expansions when R, Q increasing are also made a evident by Fig. 15.

Figs. 16–18 compare five significant theories of thin and thick plates for $R = Q = 50$. LM4 analysis is

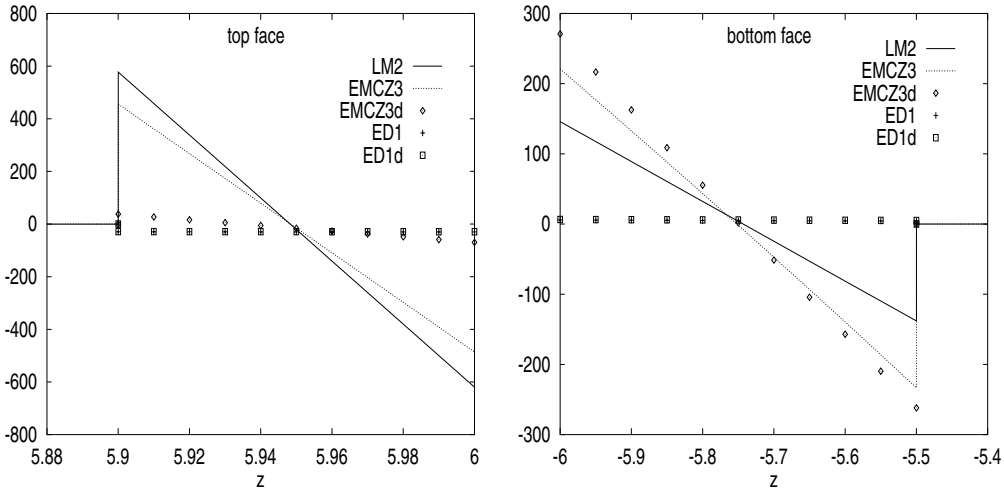

Fig. 11. BM3: in-plane stresses distribution $\overline{S}_{xx}$ in the two sandwich faces. Comparison among five significant theories ($R = Q = 25$).

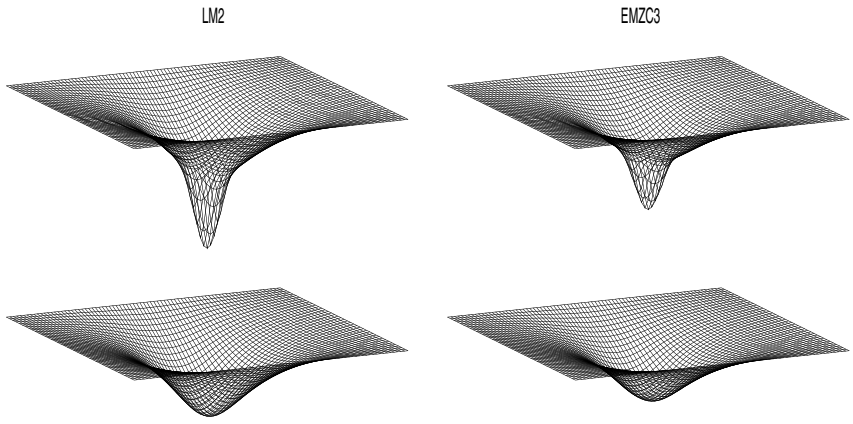

Fig. 12. BM3: deformed faces (top and bottom) for LM2 and EMZC3 analyses ($R = Q = 25$).

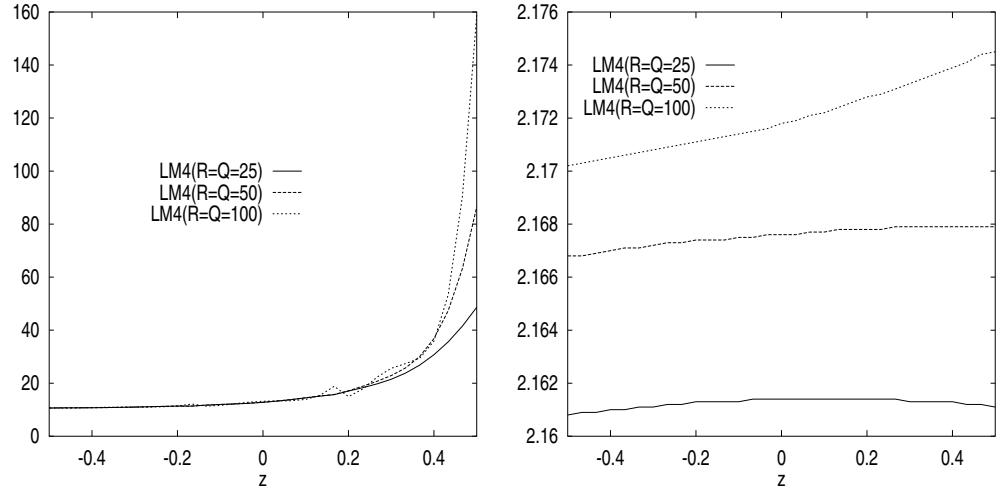

Fig. 13. BM4: effect of R and Q on trough-the-thickness distribution of transverse displacement $U_z'(a/2, b/2)$. Comparison between thick ($a/h = 4$, left) and thin ($a/h = 100$, right) plates.

Table 7
BM4: transverse displacements $U'_z(a/2, b/2, 0)$ and in-plane stress $S'_{xx}(a/2, b/2, h/2)$

a/h	U'_z			S'_{xx}		
	4	10	100	4	10	100
$R = Q = 25$						
LM4	12.778	4.638	2.161	106.61	27.42	5.62
EMZC3	11.286	4.597	2.161	40.738	17.51	5.63
EMZC3d	16.29	4.796	2.129	12.85	9.77	5.60
ED4	12.341	4.416	2.157	48.02	18.75	5.59
ED1	13.888	4.081	2.116	3.98	4.49	5.236
$R = Q = 50$						
LM4	12.781	4.699	2.168	238.84	74.536	7.0965
EMZC3	9.167	4.546	2.167	68.653	33.088	7.0919
EMZC3d	18.197	5.109	2.135	15.913	12.703	6.938
ED4	13.446	4.488	2.163	86.127	37.762	7.0417
ED1	15.768	4.384	2.121	4.525	5.0312	5.928
$R = Q = 100$						
LM4	13.188	4.696	2.172	477.83	185.85	10.417
EMZC3	6.362	4.247	2.172	106.30	59.259	9.963
EMZC3d	20.209	5.433	2.139	19.178	15.927	8.913
ED4	16.037	4.608	2.167	137.97	72.749	9.987
ED1	17.759	4.703	2.125	5.104	5.607	6.580

Table 8
BM4: transverse shear and normal stresses $S'_{xz}(0, b/2, 0)$ and $S'_{zz}(a/2, b/2, h/2)$

a/h	S'_{xz}			S'_{zz}		
	4	10	100	4	10	100
$R = Q = 25$						
LM4	0.222	0.121	0.0140	42.36	6.794	0.0676
EMZC3	0.209	0.121	0.0140	42.22	6.792	0.0679
EMZC3d	0.256	0.129	0.0139	42.61	6.816	0.0679
ED4	0.146	0.109	0.0143	42.25	6.760	0.0676
ED1	0.354	0.151	0.0149	42.25	6.760	0.0676
$R = Q = 50$						
LM4	0.205	0.116	0.0131	156.39	25.099	0.250
EMZC3	0.205	0.112	0.0130	155.71	25.023	0.252
EMZC3d	0.256	0.129	0.0130	157.64	25.214	0.252
ED4	0.0822	0.0854	0.0133	156.25	25	0.25
ED1	0.354	0.151	0.0147	156.25	25	0.25
$R = Q = 100$						
LM4	0.290	0.119	0.00925	630.21	100.09	1.0022
EMZC3	0.241	0.123	0.00935	621.90	99,736	1.0074
EMZC3d	0.188	0.101	0.00913	630.62	100.88	1.008
ED4	0.456	0.175	0.00943	625	100	1
ED1	0.169	0.0768	0.00697	625	100	1

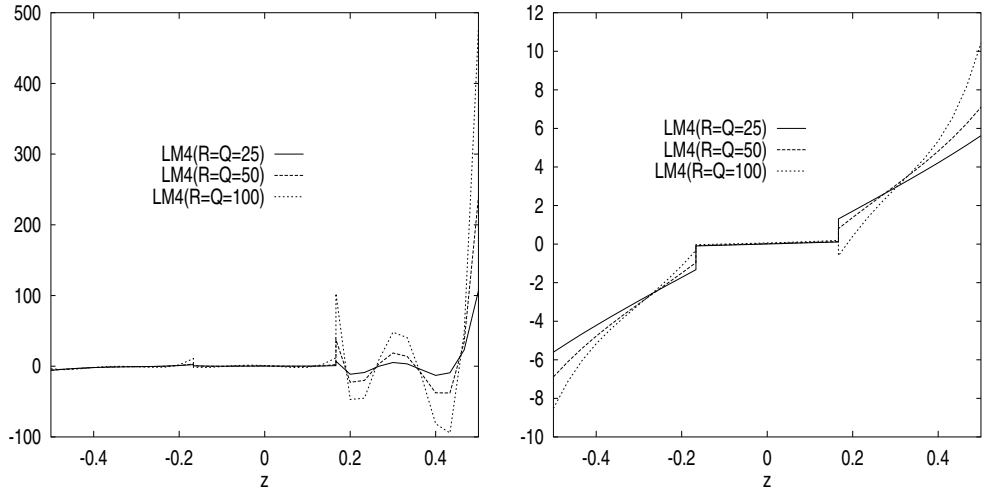

Fig. 14. BM4: effect of R and Q on trough-the-thickness distribution of in-plane stress $S'_{xx}(a/2, b/2)$. Comparison between thick ($a/h = 4$, left) and thin ($a/h = 100$, right) plates.

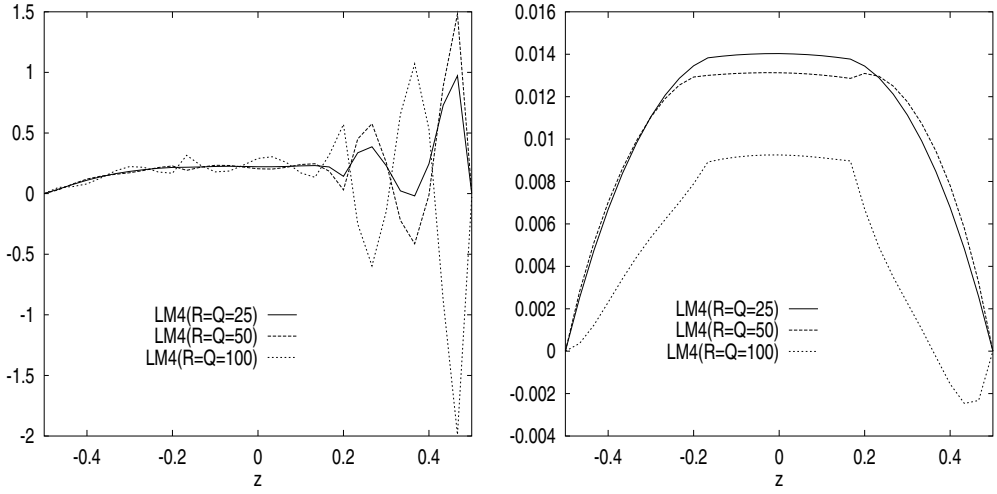

Fig. 15. BM4: effect of R and Q on trough-the-thickness distribution of transverse shear stress $S'_{xz}(0, b/2)$. Comparison between thick ($a/h = 4$, left) and thin ($a/h = 100$, right) plates.

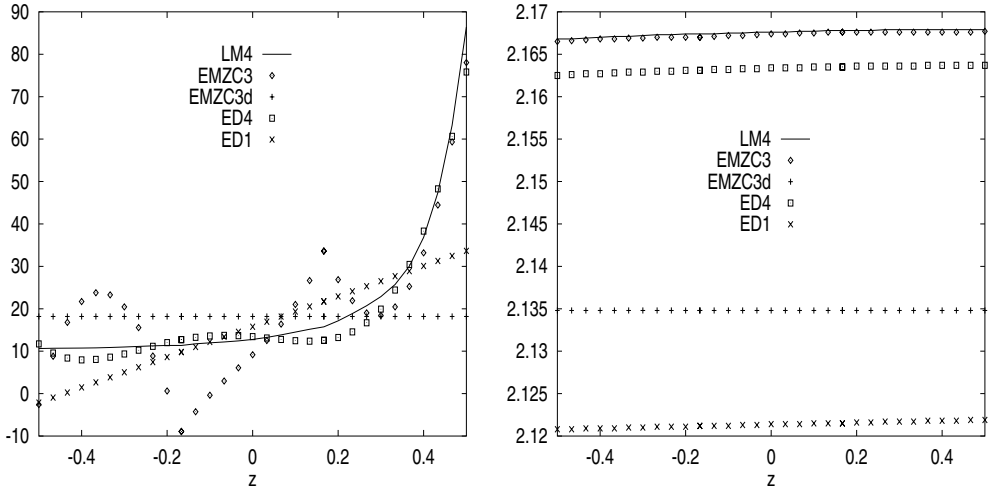

Fig. 16. BM4: trough-the-thickness distribution of transverse displacement $U'_z(a/2, b/2)$ for five significant plate theories. Comparison between thick ($a/h = 4$, left) and thin ($a/h = 100$, right) plates ($R = Q = 50$).

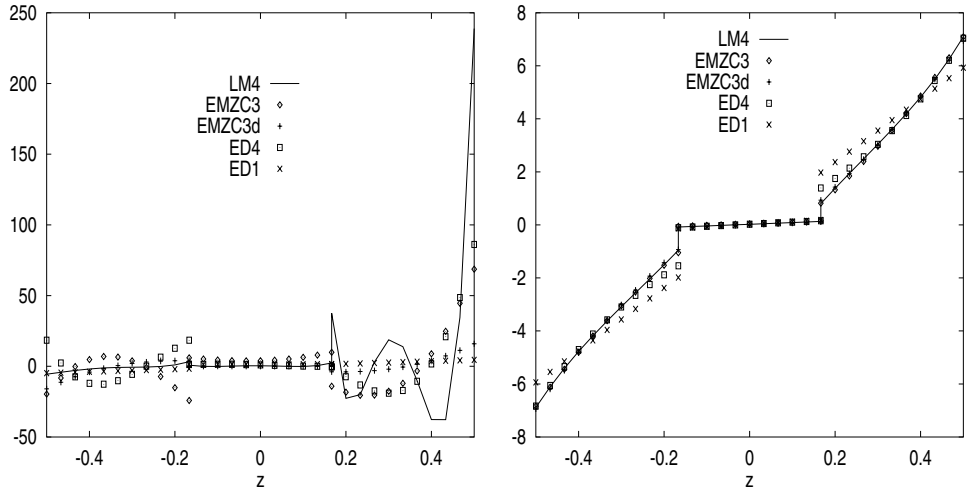

Fig. 17. BM4: trough-the-thickness distribution of in-plane stresses $S'_{xx}(a/2, b/2)$ for five significant plate theories. Comparison between thick ($a/h = 4$, left) and thin ($a/h = 100$, right) plates ($R = Q = 50$).

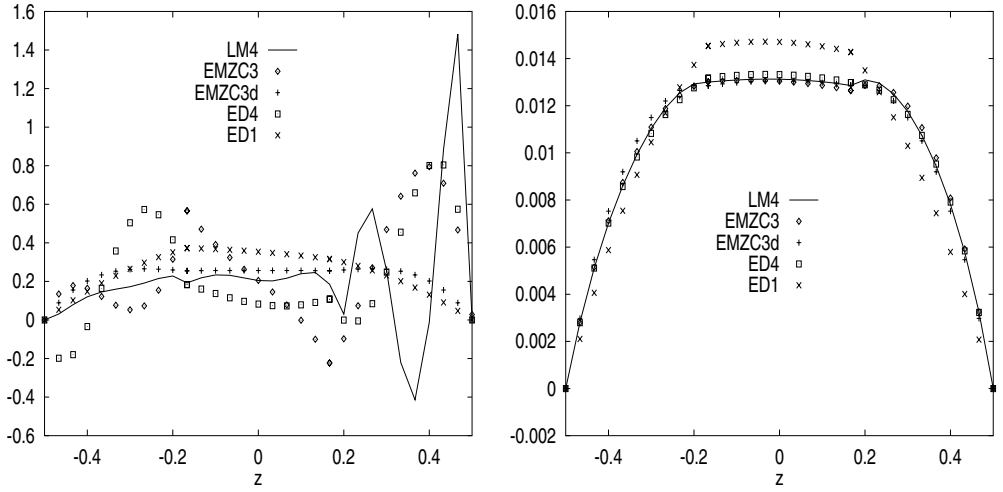

Fig. 18. BM4: trough-the-thickness distribution of transverse shear stress $S'_{xz}(0, b/2)$ for five significant plate theories. Comparison between thick ($a/h = 4$, left) and thin ($a/h = 100$, right) plates ($R = Q = 50$).

capable of capturing the singularity. The differences among the various theories increase when approaching the point in which P_z is applied. A comparison between the EMZC3d and EMZC3 results underlines the fundamental effects of transverse normal strains. These strains, being smaller, become difficult to capture in the case of thin plates.

7. Conclusions

This paper has compared various plate theories to trace the response of multilayered plates subjected to localized loadings. Closed form solutions have been discussed by considering PVD and RMVT applications and by expanding localized loading, in terms of appropriate Fourier series. The following main conclusions can be made:

1. Thin, stiff faces make sandwich plates (BM1, BM2, BM3) difficult to model when using 2D plate theories. Large errors are obtained even though very accurate ESLM theories, such as EMZC3 which describes IC and ZZ, are employed. Layer-wise analyses are required to accurately predict displacement and stress distributions.
2. An accurate prediction of the effect of localized loading, such as the BM2 and BM3 cases, requires an accurate description of transverse normal strain effect, which plays a fundamental role in capturing the localized bending of the loaded face.

3. The point load problem (BM4) has shown the capability of the LM4 analysis to capture the singularities of stress and displacement with corresponding to the loaded point of the plate. The description of the transverse strain plays a predominant role in this case. These strains, being smaller, become difficult to capture in the thin plate case.
4. The reported closed form solutions could be used as a benchmarks to assess approximated solution methods, such as finite element and boundary element methods, to describe local stress/strain states.

References

[1] Lekhnitskii SG. In: Tsai SW, Cheron T, editors. Anisotropic plates. 2nd ed. Gordon and Breach; 1968. Translated from the 2nd Russian.
[2] Ambartsumian SA. In: Ashton JE, editor. Theory of anisotropic plates. Tech Pub Co; 1969. Translated from Russian by T Cheron.
[3] Reddy JN. Mechanics of laminated composite plates, theory and analysis. CRC Press; 1997.
[4] Carrera E. Theories and finite elements for multilayered anisotropic, composite plates and shells. Arch Comput Meth Eng, State of the art Rev 2002;9:87–140.
[5] Librescu L, Reddy JN. A critical review and generalization of transverse shear deformable anisotropic plates, Euromech Colloquium 219, Kassel, September 1986. In: Elishakoff, Irretier, editors. Refined dynamical theories of beams, plates and shells and their applications. Berlin: Springer-Verlag; 1987. p. 32–43.
[6] Grigolyuk EI, Kulikov GM. General directions of the development of theory of shells. Mekh Kompoz Mater 1988;24:287–98.
[7] Kapania RK, Raciti S. Recent advances in analysis of laminated beams and plates. Am Inst Aeronaut Astronaut J 1989;27:923–46.
[8] Vasiliev VV, Lur'e SA. On refined theories of beams, plates and shells. J Compos Mater 1992;26:422–30.
[9] Noor AK, Burton WS. Assessment of shear deformation theories for multilayered composite plates. Appl Mech Rev 1989;41:1–18.
[10] Noor AK, Burton SW, Bert CW. Computational model for sandwich panels and shells. Appl Mech Rev 1996;49:155–99.
[11] Jemlelita G. On kinematical assumptions of refined theories of plates: a survey. J Appl Mech 1990;57:1080–91.
[12] Reddy JN, Robbins DH. Theories and computational models for composite laminates. Appl Mech Rev 1994;47:147–65.
[13] Lur'e SA, Shumova NP. Kinematic models of refined theories concerning composite beams, plates and shells. Int Appl Mech 1996;32:422–30.
[14] Grigorenko YaM, Vasilenko AT. Solution of problems and analysis of the stress strain state of non-uniform anisotropic shells (survey). Int Appl Mech 1997;33:851–80.
[15] Altenbach H. Theories for laminated and sandwich plates. A review. Int Appl Mech 1998;34:243–52.
[16] Carrera E. Developments, ideas and evaluations based upon the Reissner's mixed theorem in the modeling of multilayered plates and shells. Appl Mech Rev 2001;54:301–29.
[17] Carrera E. Historical review of zig-zag theories for multilayered plates and shells. Appl Mech Rev 2003;56:287–308.
[18] Carrera E. Theories and finite elements for multilayered plates and shells: a unified compact formulation with numerical assessment and benchmarking. Arch Comput Meth Eng, State of the art Rev 2003;10:215–96.
[19] Pagano NJ. Exact solutions for composite laminates in cylindrical bending. J Compos Mater 1969;3:398–411.
[20] Pagano NJ. Exact solutions for rectangular bidirectional composites and sandwich plates. J Compos Mater 1970;4:20–34.
[21] Meyer-Piening HR, Stefanelli R. Stresses, deflections, buckling and frequencies of a cylindrical curved rectangular sandwich panelbased on the elasticity solutions. In: Proceedings of the Fifth International Conference On Sandwich Constructions, Zurich, Switzerland, September 5–7, vol. II, 2000, p. 705–16.
[22] Meyer-Piening HR. Experiences with 'Exact' linear sandwich beam and plate analyses regarding bending, instability and frequency investigations. In: Proceedings of the Fifth International Conference On Sandwich Constructions, Zurich, Switzerland, September 5–7, vol. I, 2000, p. 37–48.
[23] Anderson T, Madenci E, Burton SW, Fish JC. Analytical solutions of finite-geometry composite panels under transient surface loadings. Int J Solids Struct 1998;35:1219–39.
[24] Barut A, Anderson T, Madenci E, Tessler A. A complete stress field in thick sandwich construction via single-layer theory. In: Proceedings of the Fifth International Conference on Sandwich Constructions, Zurich, Switzerland, September 5–7, vol. II, 2000, p. 691–704.
[25] Carrera E, Demasi L. Two benchmarks to assess two-dimensional theories of sandwich, composite plates. Am Inst Aeronaut Astronaut J 2003;41:1356–62.
[26] Reissner E. On a certain mixed variational theory and a proposed applications. Int J Numer Meth Eng 1984;20:1366–8.
[27] Murakami H. Laminated composite plate theory with improved in-plane response. J Appl Mech 1986;53:661–6.
[28] Carrera E, Demasi L. Multilayered finite plate element based on Reissner mixed variational theorem. Part I: theory and Part II: numerical analysis. Int J Numer Meth Eng 2002;55:191–231, p. 253–91.